OFFICE OF NAVAL RESEARCH

CONTRACT NO. N00014-86-K-0545

TECHNICAL REPORT NO. 13

AMMONIA DECOMPOSITION ON SILICON SUFACES STUDIED USING TRANSMISSION FTIR SPECTROSCOPY

A.C. Dillon, P.Gupta, M.B. Robinson A.S. Bracker and S.M. George

Submitted to

Journal of Vacuum Science Technology

SECURITY CLASSIFICATION OF THIS PAGE

AD-A226-625

REPORT DOCUMENTATION PAGE

1a. REPORT SECURITY CLASSIFICATION Unclassified	1b. RESTRICTIVE MARKINGS
2a. SECURITY CLASSIFICATION AUTHORITY	3. DISTRIBUTION / AVAILABILITY OF REPORT Approved for public release: Distribution unlimited
2b. DECLASSIFICATION / DOWNGRADING SCHEDULE	
4. PERFORMING ORGANIZATION REPORT NUMBER(S) Technical Report No. 13	5. MONITORING ORGANIZATION REPORT NUMBER(S) 13
6a. NAME OF PERFORMING ORGANIZATION Department of Chemistry Stanford University 6b. OFFICE SYMBOL (If applicable)	7a. NAME OF MONITORING ORGANIZATION Office of Sponsored Projects Stanford University
6c. ADDRESS (City, State, and ZIP Code) Stanford, California 94305-5080	7b. ADDRESS (City, State, and ZIP Code) Stanford, California 94305
8a. NAME OF FUNDING / SPONSORING ORGANIZATION Office of Naval Research 8b. OFFICE SYMBOL (If applicable)	9. PROCUREMENT INSTRUMENT IDENTIFICATION NUMBER N00014-86-K-0545
8c. ADDRESS (City, State, and ZIP Code) Chemistry Division 800 N. Quincy Street Arlington, VA 22217-5000	10. SOURCE OF FUNDING NUMBERS PROGRAM ELEMENT NO. / PROJECT NO. / TASK NO. / WORK UNIT ACCESSION NO.

11. TITLE (Include Security Classification)
Ammonia Decomposition on Silicon Surfaces Stu[illegible]ed using Transmission FTIR Spectroscopy

12. PERSONAL AUTHOR(S)
A.C. Dillon, P. Gupta, M.B. Robinson, A.S. Bracker and S.M. George

13a. TYPE OF REPORT	13b. TIME COVERED	14. DATE OF REPORT (Year, Month, Day)	15. PAGE COUNT
Interim/Technical	FROM _____ TO _____	90/31/07	

16. SUPPLEMENTARY NOTATION
EU CM

17. COSATI CODES			18. SUBJECT TERMS (Continue on reverse if necessary and identify by block number)
FIELD	GROUP	SUB-GROUP	
			< or =

19. ABSTRACT (Continue on reverse if necessary and identify by block number)

Fourier Transform Infrared (FTIR) transmission spectroscopy was used to monitor the decomposition of NH_3 and ND_3 on silicon surfaces. Experiments were performed in-situ in an ultra-high vacuum (UHV) chamber using high surface area porous silicon samples. The FTIR spectra revealed that NH_3 (ND_3) dissociatively adsorbs at 300 K to form SiH (SiD) and $SiNH_2$ ($SiND_2$) surface species. A comparison of the vibrational absorbances for the $SiNH_2$ and Si_2NH surface species indicated that the Si_2NH species could account for $\leq$11% of the surface coverage at 300 K. The infrared absorbances of the SiN-H_2 (SiN-D_2) scissors mode at 1534 cm^{-1} (1157 cm^{-1}), the Si-H (Si-D) stretch at 2077 cm^{-1} (1510 cm^{-1}) and the Si_3-N stretches at 930 and 750 cm^{-1} were employed to monitor the decomposition of the $SiNH_2$ ($SiND_2$) surface species. As the silicon surface was annealed to 700 K, the FTIR spectra revealed that the $SiNH_2$ ($SiND_2$) surface species gradually decomposed to produce Si_3N species and additional SiH species. Above 680 K, the SiH surface species decreased concurrently with the desorption of H_2 from the porous silicon surface. The uptake of surface species at various adsorption temperatures was

CONTINUED ON REVERSE SIDE

20. DISTRIBUTION / AVAILABILITY OF ABSTRACT	21. ABSTRACT SECURITY CLASSIFICATION
☒ UNCLASSIFIED/UNLIMITED ☐ SAME AS RPT. ☐ DTIC USERS	Unclassified

22a NAME OF RESPONSIBLE INDIVIDUAL	22b. TELEPHONE (Include Area Code)	22c. OFFICE SYMBOL
Dr. David L. Nelson / Dr. Mark Ross	(202) 696-4410	

DD FORM 1473, 84 MAR 83 APR edition may be used until exhausted. All other editions are obsolete.

SECURITY CLASSIFICATION OF THIS PAGE

19. also monitored as a function of NH_3 (ND_3) exposure time.. These studies revealed that similar results were obtained after NH_3 (ND_3) was adsorbed to saturation coverage at a particular adsorption temperature and after the surface was annealed to the same temperature following a saturation NH_3 (ND_3) exposure at 300 K.

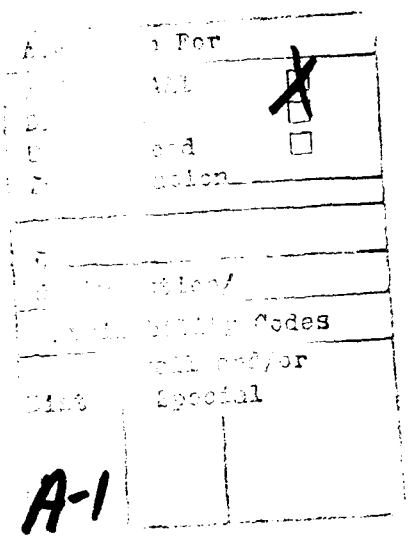

(Submitted to J. Vac. Sci. Technol.)

Ammonia Decomposition on Silicon Surfaces Studied Using Transmission FTIR Spectroscopy

A.C. Dillon, P. Gupta, M.B. Robinson, A.S. Bracker and S.M. George

Department of Chemistry
Stanford University
Stanford, California 94305

Abstract

Fourier Transform Infrared (FTIR) transmission spectroscopy was used to monitor the decomposition of NH_3 and ND_3 on silicon surfaces. Experiments were performed *in-situ* in an ultra-high vacuum (UHV) chamber using high surface area porous silicon samples. The FTIR spectra revealed that NH_3 (ND_3) dissociatively adsorbs at 300 K to form SiH (SiD) and $SiNH_2$ ($SiND_2$) surface species. A comparison of the vibrational absorbances for the $SiNH_2$ and Si_2NH surface species indicated that the Si_2NH species could account for $\leq 11\%$ of the surface coverage at 300 K. The infrared absorbances of the SiN-H_2 (SiN-D_2) scissors mode at 1534 cm^{-1} (1157 cm^{-1}), the Si-H (Si-D) stretch at 2077 cm^{-1} (1510 cm^{-1}) and the Si_3-N stretches at 930 and 750 cm^{-1} were employed to monitor the decomposition of the $SiNH_2$ ($SiND_2$) surface species. As the silicon surface was annealed to 700 K, the FTIR spectra revealed that the $SiNH_2$ ($SiND_2$) surface species gradually decomposed to produce Si_3N species and additional SiH species. Above 680 K, the SiH surface species decreased concurrently with the desorption of H_2 from the porous silicon surface. The uptake of surface species at various adsorption temperatures was also monitored as a function of NH_3 (ND_3) exposure time. These studies revealed that similar results were obtained after NH_3 (ND_3) was adsorbed to saturation coverage at a particular adsorption temperature and after the surface was annealed to the same temperature following a saturation NH_3 (ND_3) exposure at 300 K.

I. Introduction

The adsorption of ammonia on silicon surfaces is a fundamentally and technologically important surface reaction. The details of NH_3 adsorption are critical for an understanding of chemisorption on silicon surfaces. The adsorption and decomposition of ammonia on silicon surfaces also plays a key role in semiconductor device processing because NH_3 is employed to grow silicon nitride layers for dielectric insulation.

A wide variety of techniques have been used to monitor the reaction of NH_3 on silicon surfaces. For example, scanning tunneling microscopy (STM) (1-5), high-resolution electron-energy-loss spectroscopy (HREELS) (6-8), ultraviolet photoelectron spectroscopy (UPS) (9-11), X-ray photoelectron spectroscopy (XPS) (10-12), temperature programmed desorption (TPD) (13,14), electron-stimulated desorption ion angular distributions (ESDIAD) (14,15) and laser induced desorption (LID) (13) have been employed to study NH_3 on Si(111)(7x7), Si(100)(2x1) and Si(111)(2x1). This research has attempted to determine whether the adsorption of NH_3 on silicon surfaces is dissociative or nondissociative.

Older HREELS (8) and UPS (9) experiments suggested that the chemisorption of ammonia on Si(111)(7x7) at room temperature was nondissociative. A recent HREELS study also provided evidence that NH_3 is adsorbed primarily as a nondissociated molecule at room temperature on Si(111)(2x1) (7). However, more recent HREELS studies have observed the dissociative adsorption of NH_3 on Si(111)(7x7) (6). Recent UPS/XPS studies are also consistent with dissociative NH_3 adsorption on Si(100)(2x1) and Si(111)(7x7) (11).

Recent investigations have begun to probe the extent of NH_3 dissociation and determine the NH_3 dissociation products. STM studies suggested the presence of two surface species for ammonia adsorption on Si(111)(7x7) (5). XPS and UPS studies have argued that NH_3 dissociates to form Si_2NH on Si(100)(2x1) (11). In contrast, TPD and ESDIAD studies have evidence that $SiNH_2$ and SiH are the major decomposition products on Si(100)(2x1)

(14). Recent XPS, ISS and STM studies on Si(100)2x1 are consistent with the complete dissociation of NH_3 upon adsorption for temperatures as low as 90 K (2,3).

Fourier transform infrared (FTIR) spectroscopy is sensitive to surface molecular structure and can resolve closely-spaced vibrational features. Transmission FTIR studies can also probe the infrared region below 1200 cm^{-1} that is obscured in multiple total-internal-reflection experiments because of silicon lattice absorption (16-18). Numerous low frequency vibrational modes in this infrared region yield valuable structural information. Because typical infrared cross sections are $\sigma \approx 1x10^{-18}$ cm^2 (19), sensitivity requirements limit transmission FTIR studies to high surface area materials. Single crystal samples with approximately $1x10^{15}$ surface atoms/cm^2 do not provide the necessary surface area.

Porous silicon can be utilized to obtain high-surface area, crystalline silicon samples. Porous silicon was first obtained by Uhlir (20) and Turner (21) by anodizing single-crystal silicon in dilute hydrofluoric acid. Transmission electron microscopy (TEM) micrographs have shown that porous silicon made from *p*-doped silicon contains a network of nearly parallel pores approximately 20-100 Å in diameter with a center-to-center separation of approximately the same magnitude (22). This porous network generates a surface area of approximately 200 m^2/cm^3 as shown by Brunauer-Emmett-Teller (BET) model methods (23).

Additional material properties of porous silicon have been recently reported (24-27). When prepared under ordinary conditions, porous silicon retains the crystallinity of the original silicon wafer (28-30). The crystallinity of porous silicon allows epitaxial layers of silicon to be grown on porous silicon using molecular beam epitaxy (MBE) techniques (31). Porous silicon also exhibits sharp and pronounced infrared absorption features that can be assigned unambiguously to silicon monohydride and dihydride surface species (32). The desorption kinetics of H_2 from monohydride (SiH) and dihydride (SiH_2) species on porous silicon have recently been measured (32). These H_2 desorption kinetic studies were in excellent agreement

with the desorption kinetics of H_2 from Si(111)7x7 single crystal surfaces (33,34).

Porous silicon has also been used recently to study the adsorption and decomposition of H_2O on silicon surfaces (35). This study identified SiOH as the surface species following the dissociative adsorption of H_2O at 300 K. The decomposition of SiOH surface species and subsequent growth of SiH species was observed between 400 - 600 K. The decomposition of SiOH on porous silicon surfaces was in extremely good agreement with earlier laser induced desorption (LID) studies of the thermal stability of SiOH species on Si(111)7x7 (36,37).

In this study, the nature of ammonia species adsorbed on porous silicon surfaces was examined using transmission FTIR vibrational spectroscopy. The FTIR spectra revealed that ammonia dissociatively adsorbs on silicon surfaces at 300 K and produces $SiNH_2$ and SiH surface species. The thermal stability of the surface reaction species was then measured by monitoring the Si-H (Si-D) stretch, the $SiN-H_2$ ($SiN-D_2$) scissors mode, and the Si_3-N stretches. These temperature-dependent FTIR studies revealed that the $SiNH_2$ surface reaction intermediate decomposed to Si_3N and SiH surface species between 400 - 700 K. In addition, the growth of surface species at various adsorption temperatures was examined as a function of NH_3 (ND_3) exposure time. The results from the annealing studies and the uptake experiments were in excellent agreement.

II. Experimental

A. Preparation of Porous Silicon

The electrochemical techniques used to prepare porous silicon have been previously described (32). These studies employed single-crystal Si(100) wafers with a thickness of 400 μm. These samples were *p*-type boron-doped with a resistivity of $\rho = 0.20\ \Omega cm$. The electrolyte consisted of a 38% hydrofluoric acid-ethanol mixture. The anodization reaction was performed for 15 s with a constant current of 200 mA/cm^2. This current flux and time corresponded to a total charge of 1.12 C/cm^2.

In agreement with previous studies (29,32), the porous samples produced using the above conditions were bluish-gray in color. Optical micrographs of cross-sections of the anodized Si(100) wafers determined that the thickness of the porous layer was 2 μm. Given a surface area of 200 m^2/cm^3, the 2 μm thick porous silicon layer provided a surface area enhancement of x400 compared with a single-crystal sample.

B. UHV Chamber for Transmission FTIR Studies

Prior to mounting the porous silicon sample in the UHV chamber, the sample was rinsed successively in ethanol, trichloroethylene and hydrofluoric acid. The hydrofluoric acid was used to remove any native oxide that may have formed on the porous silicon surfaces after anodization. The samples were then mounted at the bottom of a liquid-nitrogen-cooled cryostat on a differentially-pumped rotary feedthrough (38). The crystal mounting design and techniques for sample heating have been described previously (32).

The UHV chamber for *in-situ* transmission FTIR studies was similar to the UHV chamber employed earlier (32). The UHV chamber was pumped by a 190 l/sec Balzers turbomolecular pump that was backed by another 50 l/sec turbomolecular pump. This tandem turbomolecular pump enabled pressures of 1-2 x 10^{-8} Torr to be obtained within 2 hr. after breaking vacuum. An isolation valve between the sample introduction chamber and the rest of the chamber facilitated this rapid recovery time after changing samples.

A Nicolet 740 FTIR spectrometer and an MCT-B infrared detector were employed in these studies. The infrared beam passed through a pair of 0.5 inch thick CsI windows on the vacuum chamber. Lower infrared frequencies were transmitted and higher optical throughput was obtained with CsI windows compared with the earlier ZnSe windows (32). The O-ring seals on the CsI salt windows limited the typical operating pressures to 8 x 10^{-9} Torr.

C. Adsorption and Thermal Annealing Experiments

The surface species produced during NH_3 (ND_3) adsorption were studied as a function of ammonia exposure and silicon surface temperature. In these experiments, the silicon substrate was held at a constant temperature. FTIR spectra were recorded versus ammonia exposure until a saturation coverage was obtained. Adsorption as a function of NH_3 (ND_3) exposure time was measured at isothermal temperatures of 300, 400, 600 and 800 K. The FTIR spectra were monitored at the adsorption temperature for the isothermal measurements at 300 and 400 K. Because of increased infrared absorption by free carriers at higher temperatures (39-41), FTIR spectra were recorded at 500 K for the isothermal measurements at 600 K and 800 K.

For the thermal annealing studies, porous silicon samples at 300 K were exposed to NH_3 (ND_3) until a saturation coverage was obtained. NH_3 (ND_3) exposures at 1×10^{-5} Torr for 30 minutes were employed to achieve a saturation coverage. The silicon surface temperature was then increased using a heating rate of 7 K/sec. The sample was held at the annealing temperature for one minute. Subsequently, the sample was returned to the initial temperature of 300 K before recording the FTIR spectra. This experimental sequence was performed repeatedly for annealing temperatures up to 860 K.

A new porous silicon sample prepared under identical conditions was used for each set of annealing experiments. The total concentrations of monohydride and dihydride species initially present on the porous silicon surface were the same within ±5% for each sample. To obtain a clean surface before ammonia exposure, the porous silicon sample was annealed in vacuum to remove the surface hydrogen. This procedure consisted of annealing the porous silicon at 640 K for 4 minutes, followed by annealing at 800 K for an additional 4 minutes. Previous hydrogen desorption studies have shown that this annealing procedure is sufficient to remove hydrogen from both surface monohydride and dihydride species (32).

III. Results

The spectra of porous silicon after saturation NH_3 and ND_3 exposures at 300 K are shown in Figs. 1 and 2, respectively. After a NH_3 saturation exposure, the porous silicon spectra in Fig. 1 exhibited pronounced infrared absorption features at 3465, 3388, 2077, 1534, 827 and 620 cm^{-1}. Minor spectral features appeared at 1102 and 770 cm^{-1}. After a ND_3 saturation exposure, the major infrared features in Fig. 2 were observed at 2594, 2483, 1510, 1157 and 782 cm^{-1}. A minor spectral feature also appeared at 827 cm^{-1}.

After a saturation ammonia exposure at 300 K, changes in the infrared absorption spectrum of porous silicon versus annealing temperature are shown in Figs. 3 and 4. Figure 3a shows the decrease in the infrared absorption of the SiN-H_2 scissors mode at 1534 cm^{-1} versus annealing from 300 - 680 K. Figure 3b shows the concurrent increase in the absorption of the Si-H stretch at 2077 cm^{-1} over the same temperature range. At high temperatures, the Si-H absorption band broadens and blue shifts to 2102 cm^{-1}. This effect is attributed to SiH species which are backbonded to nitrogen atoms and is consistent with previous vibrational studies of NH_3 decomposition on Si(111)(7x7) (6).

Figure 4 shows the growth of infrared absorption features at 1088, 930 and 750 cm^{-1} associated with Si_3-N vibrational modes versus annealing from 680 - 860 K. A Si-H bending feature following NH_3 adsorption overlaps with the Si_3-N feature at 750 cm^{-1}. Consequently, the spectra shown in Fig. 4 were obtained after a saturation ND_3 exposure. By 860 K, the absorption features at 930 and 750 cm^{-1} broaden and shift to 943 and 790 cm^{-1} as a greater number of nitrogen atoms are incorporated into the silicon lattice.

The integrated infrared absorbances versus annealing temperature after saturation NH_3 and ND_3 exposures at 300 K are displayed in Fig. 5 and Fig. 6, respectively. An increase by nearly a factor of 2 in the integrated absorbance for the Si-H and Si-D stretching vibrations is observed as the temperature is increased from 300 K - 680 K. At temperatures higher than 680 K, the integrated absorbance decreases for both Si-H and Si-D stretching

vibrations. This decrease is consistent with the desorption of H_2 or D_2 from the silicon surface (32-34).

Figures 5 and 6 also reveal that the SiN-H_2 and SiN-D_2 scissors vibrational modes corresponding to $SiNH_2$ and $SiND_2$ surface species have disappeared from the FTIR spectrum after annealing above 680 K. The decrease in the integrated absorbances for the SiN-H_2 and SiN-D_2 scissors modes is correlated with the increase in the absorbance of the Si-H and Si-D stretching vibrations. In addition, an increase in the infrared absorbances at 1088, 930 and 750 cm^{-1} associated with Si_3-N vibrational modes is observed from 500 to 850 K. The increase in the absorbance of the Si_3N species is concurrent with the increase in the absorbance of the SiH surface species.

The integrated absorbances of the Si-D stretching vibration versus ND_3 exposure at 300, 400 and 600 K are displayed in Fig. 7. ND_3 dissociative chemisorption as measured by the SiD surface species is characterized by a rapid initial ND_3 adsorption. This rapid adsorption rate is then followed by progressively decreasing adsorption rates that ultimately lead to a saturation coverage after large ND_3 exposures. Figure 7 reveals that the saturation deuterium coverage is very dependent on surface temperature. The saturation deuterium coverage at 600 K is larger than the saturation deuterium coverage obtained at 300 K by a factor of approximately 1.8.

Figure 8 shows the growth of the integrated absorbance of the SiN-D_2 scissors mode versus ND_3 exposure at 300, 400 and 600 K. The uptake of $SiND_2$ surface species is again characterized by a fast initial adsorption step. Like the results for the Si-D stretching vibration shown in Fig. 7, the integrated absorbance of the SiN-D_2 scissors mode saturates after large ND_3 exposures. The saturation coverage of $SiND_2$ species obtained at 600 K is significantly smaller than the saturation coverage of $SiND_2$ species obtained at 300 K.

IV. Discussion

A. Infrared Spectrum after Ammonia Exposure

Reflectance infrared studies of hydrogen on Si(100) have assigned infrared features between 2100 and 2080 cm^{-1} to Si-H stretching vibrations (42,43). Upon anodization, porous silicon exhibits two absorption peaks between 2087 - 2110 cm^{-1}. Thermal annealing studies have assigned these two absorption features to silicon dihydride and silicon monohydride stretching vibrations (32). The presence of silicon dihydride on anodized porous silicon is also confirmed by the SiH_2 scissor mode at 910 cm^{-1} (32). As the dihydride is removed from the surface, the monohydride peak at 2110 cm^{-1} shifts to 2102 cm^{-1} (32).

The spectrum in Fig. 1 was obtained after the desorption of hydrogen and subsequent NH_3 exposure at 300 K. Figure 1 does not show any infrared absorption from a possible SiH_2 scissors mode at 910 cm^{-1}. This absence suggests that the 2077 cm^{-1} feature after the NH_3 saturation exposure at 300 K is produced by a silicon-monohydride species. The corresponding infrared absorption at 620 cm^{-1} is assigned to the deformation mode of the SiH species. This assignment is in agreement with previous infrared studies on porous silicon (32) and HREELS investigations on Si(100)(2x1) (44). The infrared feature at 1510 cm^{-1} in Fig. 2 after ND_3 exposure at 300 K is consistent with a Si-D stretching vibration. The Si-D deformation mode would be at 480 cm^{-1} which is below the lower frequency limit of the MCT-B infrared detector.

Previous infrared studies of R_3SiNH_2 have observed absorption features between 3474 - 3484 cm^{-1} and 3401 - 3404 cm^{-1} that have been attributed to the $SiN-H_2$ asymmetric and symmetric stretching modes, respectively (45,46). HREELS studies of ammonia adsorption on Si(111)(7x7) have assigned an energy loss feature at 3402 cm^{-1} to the $SiN-H_2$ symmetric stretching vibration (6). Consequently, the infrared features at 3465 and 3388 cm^{-1} in Fig. 1 are attributed to the $SiN-H_2$ asymmetric and symmetric stretching vibrations,

respectively. Similarly, the absorption features at 2594 and 2483 cm^{-1} in Fig. 2 are consistent with the SiN-D_2 asymmetric and symmetric stretching vibrations, respectively.

Absorption features around 1536 - 1562 cm^{-1} for R_3SiNH_2 have been previously assigned to the SiN-H_2 scissors mode (45,46). Similarly, HREELS studies of ammonia on Si(111)(7x7) have attributed energy loss features at 1516 cm^{-1} to the SiN-H_2 scissors mode (6). Therefore, the infrared feature at 1534 cm^{-1} in Fig. 1 is ascribed to the $SiNH_2$ scissors mode. The corresponding SiN-D_2 scissors mode appears at 1157 cm^{-1} in Fig. 2.

The Si-NH_2 stretching vibration of R_3SiNH_2 has been observed at 828 - 857 cm^{-1} (45). HREELS studies have also assigned the energy loss feature at 790 cm^{-1} to the Si-NH_2 stretching vibration (6). Thus the absorption feature at 827 cm^{-1} in Fig. 1 is attributed to the Si-NH_2 stretching vibration. Similarly, the absorption feature at 782 cm^{-1} in Fig. 2 is ascribed to the Si-ND_2 stretching vibration.

The infrared spectrum of porous silicon after NH_3 adsorption at 300 K is almost identical to the HREELS spectra obtained after NH_3 adsorption on Si(111)(7x7) (6). The close correspondence in infrared spectral structures and frequencies demonstrates that porous silicon surfaces are very similar to single-crystal silicon surfaces. This similarity suggests that high surface area porous silicon surfaces can be employed to study silicon surface chemistry.

B. Si-NH_2 versus Si_2NH Surface Species

Infrared studies of $[(R_3)Si]_2NH$ species have assigned absorption features appearing from 1159 - 1179 cm^{-1} to the Si_2N-H out-of-plane deformation mode (45,47,48). The in-plane deformation mode has been attributed to absorption features appearing between 754 - 788 cm^{-1} (45). There are weak infrared absorption features appearing at 1102 cm^{-1} and 770 cm^{-1} in Fig. 1 that approach the detection limits of this experiment. These features are assigned to the out-of-plane and in-plane deformation modes of the Si_2NH species, respectively. A minor absorption feature also appears as a shoulder at 827 cm^{-1} on the major

feature at 782 cm^{-1} in Fig. 2. This absorption feature may be attributed to the out-of-plane Si_2N-D deformation mode. The corresponding Si_2N-D in-plane deformation mode would appear at approximately 560 cm^{-1} which approaches the lower frequency limit of the MCT-B infrared detector.

Figures 1 and 2 indicate that only a small population of Si_2NH species exist on the porous silicon surface after a saturation NH_3 exposure at 300 K. The majority of the nitrogen-containing surface species are $SiNH_2$. Using gas phase extinction coefficients for $[(C_2H_5)_3Si]_2NH$ and $(C_2H_5)_3SiNH_2$ (45), the relative populations of Si_2NH and $SiNH_2$ species can be estimated using the simple Beer's Law expression, $A = \epsilon cz$. In this relationship, A is the integrated absorbance, ϵ is the extinction coefficient, c is the concentration, and z is the path length.

Integrated absorbances obtained after a saturation NH_3 exposure at 300 K for the SiN-H_2 scissors mode and the Si_2N-H out-of-plane bending mode were A = .172 cm^{-1} and A $\leq$ .030 cm^{-1}, respectively. The integrated absorbance for the Si_2N-H out-of-plane bending mode is given as an upper limit because this absorbance is only slightly larger than the experimental noise. The corresponding gas phase extinction coefficients for the SiN-H_2 scissors mode and the SiN-H out-of-plane bending mode are ϵ = 78 L/mole cm and ϵ = 148 L/mole cm, respectively (45).

Upon conversion to units appropriate for this experiment, values of $\epsilon = 1.2 \times 10^8$ cm/mole and $\epsilon = 1.6 \times 10^8$ cm/mole are obtained for the SiN-H_2 scissors mode and the SiN-H out-of-plane bending mode, respectively (49). Using these values in the Beer's Law expression, 8:1 was obtained as the largest possible concentration ratio between $SiNH_2$ and Si_2NH surface species. Consequently, the Si_2NH species can account for $\leq$ 11% of all the surface species after a saturation NH_3 exposure at 300 K. This estimation assumes that the gas phase extinction coefficients for the SiN-H_2 scissors mode and the SiN-H out-of-plane bending mode can be applied on silicon surfaces.

In addition, there was no evidence for molecular NH_3 on the porous silicon surface. The NH_3 degenerate deformation mode at 1627 cm^{-1} is not observed in the infrared spectrum in Fig. 1. After a NH_3 saturation exposure at 300 K, the infrared spectra shown in Figs. 1 and 2 display clear evidence of dissociative NH_3 adsorption. The major surface species are Si-H and Si-NH_2. The small absorbance for the Si_2N-H out-of-plane bending mode indicates that Si_2NH is present only as a minor surface species.

C. Si_3N Silicon Nitride Species

The thermal annealing studies in Figs. 3-6 demonstrate that the $SiNH_2$ and $SiND_2$ surface species decompose upon annealing to 700 K. The infrared spectra in Figs. 3 and 4 and the integrated absorbance measurements in Figs. 5 and 6 reveal that the decrease in the $SiNH_2$ species is accompanied by the concurrent growth of SiH and Si_3N species. This growth is clearly observed by the increase of the absorbance of the vibrational modes associated with SiH and Si_3-N surface species.

The infrared absorption features in Fig. 4 at 1088, 930 and 750 cm^{-1} correspond to the vibrational spectra of Si_3N species. Previous infrared studies of $(R_3)SiNHSi(R_3)$ species have assigned the Si-N-Si asymmetric and symmetric stretching modes to broad infrared absorption features centered around 920 - 934 cm^{-1} and 533 - 576 cm^{-1}, respectively (45,48). Investigations of the nearly planar trisilylamine molecule $(SiH_3)_3N$ have also attributed a broad absorption feature at 996 cm^{-1} to the asymmetric Si_3N stretching mode (50).

The absorption features at 1088 and 750 cm^{-1} can not be assigned based on the frequencies of gas phase compounds. These absorption features may originate from special surface structures. For example, LEED studies of the nitridation of Si(111)(7x7) have found that clean silicon surfaces nitridated in the temperature range of 1075 K - 1300 K exhibit an ordered 8x8 pattern (51,52). HREELS experiments have observed energy losses at 1136, 734 and 483 cm^{-1} for a Si(111) surface that was nitrated at 1240 K and produced an 8x8 LEED pattern (53).

Based on the above observations, the appearance of the absorption feature at 930 cm^{-1} in Fig. 4 is attributed to an asymmetric stretching mode of Si_3N surface species. The absorption features appearing at 1088 and 750 cm^{-1} may be caused by the appearance of Si_3N surface structures that are similar to the ordered 8x8 patches. In accordance with frequencies expected for pyramidal XY_3 molecules (54), the absorption features at 1088 and 750 cm^{-1} may be attributed to the symmetric or degenerate stretching mode and the symmetric deformation mode, respectively. The low frequency absorption feature expected at approximately 483 cm^{-1} (53) occurs outside the limits of the MCT-B detector and would be attributed to the degenerate deformation mode.

D. Thermal Decomposition of $SiNH_2$ Surface Species

The decomposition of the $SiNH_2$ ($SiND_2$) species between 400 - 700 K is observed in Figs. 5 and 6. The thermal stability of the $SiNH_2$ surface species measured by these FTIR studies is in good agreement with a recent laser-induced desorption (LID) study of NH_3 decomposition on Si(111)(7x7) (13). Temperature-programmed linear-ramp LID experiments revealed that the $SiNH_2$ LID signals persisted to 700 K. The correlation between these FTIR results and the earlier LID studies is discussed in detail elsewhere (37).

Fig. 3 reveals that the SiH surface species increase as the $SiNH_2$ species decrease. The thermal annealing results in Figs. 5 and 6 show that the maximum integrated absorbance for the Si-H (Si-D) stretching vibration is reached at 660 K. At this temperature, the integrated absorbance of the Si-H (Si-D) stretching vibration is slightly less than twice the initial Si-H (Si-D) integrated absorbance at 300 K.

The increase in the integrated absorbance of Si-H (Si-D) stretching vibration suggests the reaction $SiNH_2$ --> 2SiH + Si_3N. Assuming complete dissociation to $SiNH_2$ and SiH surface species, a saturation NH_3 exposure would be expected to produce equivalent amounts of surface $SiNH_2$ and SiH species i.e., NH_3 --> SiH + $SiNH_2$. Subsequently, the

decomposition of $SiNH_2$ to SiH and Si_3N would produce an overall reaction of SiH + $SiNH_2$ --> 3SiH + Si_3N.

At the maximum absorbance at 660 K, the SiH species does not increase by a factor of three as expected. The lower increase may be attributed to a combination of effects. For example, the decomposition of a small fraction of the $SiNH_2$ surface species upon adsorption would increase the initial absorbance of the SiH surface species and lower the expected growth of the SiH surface species during $SiNH_2$ decomposition. There is evidence that a small population of Si_2NH species may be present on the surface at 300 K. This evidence is provided by the weak absorption features at 1102 and 770 cm^{-1} assigned to the Si_2N-H deformation modes.

Recent STM, XPS and ISS studies have also provided evidence for the complete dissociation of NH_3 to form silicon nitride and silicon monohydride species on Si(100)(2x1) at 90 K and at 300 K (2,3). A small growth which approaches the limits of detection in the absorption region assigned to the Si_3-N asymmetric stretching vibration is possibly discernible in Figs. 1 and 2. Consequently, a small population of Si_3N may be present on the porous silicon surfaces after a saturation NH_3 exposure at 300 K.

Desorption of NH_3 or H_2 would also lower the expected increase of the absorbance of the Si-H stretching vibration. Recent TPD studies of NH_3 adsorption on Si(100)(2x1) have reported that the recombinative desorption of molecular NH_3 at temperatures above 600 K is a minor reaction channel (14). In this FTIR study, an increase in the background pressure of NH_3 was observed by the mass spectrometer at surface temperatures above 600 K. Unfortunately, discriminating between NH_3 desorption from the porous silicon or from the copper sample holder was not possible.

The Si-H surface species may also be lost due to H_2 recombinative desorption prior to the decomposition of all the $SiNH_2$ surface species. No increase in the background pressure of H_2 could be detected by the mass spectrometer for annealing temperatures between 300 K - 640 K. This behavior is consistent with hydrogen transfer to the silicon surface during

$SiNH_2$ decomposition. However, the absorbance of the Si-H (Si-D) stretching vibration decreases as expected when H_2 (D_2) desorbs from silicon surfaces at temperatures only slightly above the maximum absorbance at 660 K (32-34).

E. Adsorption Studies

Adsorption on porous silicon is complicated because uptake into the pores is conductance-limited. However, NH_3 (ND_3) adsorption studies at various isothermal temperatures provide an interesting comparison with the annealing studies that were performed after saturation NH_3 (ND_3) exposures at 300 K. These experiments measure the effects of adsorption temperature on the resultant surface species.

The SiD uptake kinetics shown in Fig. 7 are consistent with the annealing results shown in Fig. 6. The saturation coverage of SiD species obtained at 600 K is larger than the saturation coverage at 300 K by approximately a factor of 1.8. This difference is produced by the different thermal stabilities of the $SiND_2$ species at these two temperatures. At 600 K, the $SiND_2$ species decompose to yield Si_3N and SiD species. At 300 K, the $SiND_2$ species is more stable and the deuterium remains in the $SiND_2$ species.

As displayed by the three uptake curves in Fig. 7, the dissociative chemisorption of ND_3 is characterized by a rapid initial ND_3 adsorption. Fig. 7 reveals that the initial adsorption of ND_3 is more rapid at 300 K than at 400 K. Previous studies of NH_3 adsorption on Si(111)7x7 have reported that the NH_3 sticking coefficient on Si(111)(7x7) decreases with surface temperature (13). The initial uptake of ND_3 at 300 and 400 K in Fig. 7 is consistent with a temperature-dependent sticking coefficient.

Fig. 7 also reveals that the saturation coverage of SiD species at 400 K is slightly greater than the saturation coverage at 300 K. The different thermal stabilities are more apparent in Fig. 7 than in Fig. 6 because the silicon surface was held at 300 or 400 K for the entire experiment. In contrast, the normalized integrated absorbances shown in Fig. 6 were

obtained after annealing the sample at each temperature for one minute.

The $SiND_2$ uptake kinetics shown in Fig. 8 are also consistent with the annealing results displayed in Fig. 6. The annealing and adsorption results confirm the greater stability of the $SiND_2$ surface species at low temperatures. The saturation coverage of $SiND_2$ species obtained at 300 K is greater by a factor of 6 than the saturation coverage obtained at 600 K.

Fig. 8 reveals that the initial growth of $SiND_2$ surface species on porous silicon during ND_3 exposure is more rapid at 300 K than at 400 K. This difference is again attributed to the temperature-dependent sticking coefficient of NH_3 on silicon surfaces. Fig. 8 also reveals a larger saturation coverage of $SiND_2$ species at 300 K compared with 400 K. In agreement with Fig. 7, this difference indicates fewer $SiND_2$ species have decomposed to fonn Si_3N and SiD surface species at 300 K.

V. Conclusions

Fourier Transform Infrared (FTIR) transmission spectroscopy was used to monitor the decomposition of NH_3 and ND_3 on silicon surfaces. Experiments were performed *in-situ* in an ultra-high vacuum (UHV) chamber using high surface area porous silicon samples. The FTIR spectra revealed that NH_3 (ND_3) dissociatively adsorbs at 300K to form SiH (SiD) and $SiNH_2$ ($SiND_2$) surface species.

A comparison of the vibrational absorbances for the $SiNH_2$ and Si_2NH surface species indicated that the Si_2NH species could account for $\leq 11\%$ of the surface coverage at 300 K. The infrared absorbances of the SiN-H_2 (SiN-D_2) scissors mode at 1534 cm^{-1} (1157 cm^{-1}), the Si-H (Si-D) stretch at 2077 cm^{-1} (1510 cm^{-1}) and the Si_3-N stretches at 930 and 750 cm^{-1} were employed to monitor the decomposition of the $SiNH_2$ ($SiND_2$) surface species. As the silicon surface was annealed to 700 K, the FTIR spectra revealed that the $SiNH_2$ ($SiND_2$) surface species gradually decomposed to produce Si_3N species and additional SiH species. Above 680 K, the SiH surface species decreased concurrently with the desorption of H_2 from the porous silicon surface.

The uptake of surface species at various adsorption temperatures was also monitored as a function of NH_3 (ND_3) exposure time. These experiments revealed a temperature-dependent sticking coefficient for NH_3 (ND_3) on porous silicon surfaces. These studies also demonstrated that similar results were obtained after NH_3 (ND_3) was adsorbed to saturation coverage at a particular adsorption temperature or after the surface was annealed to the same temperature following a saturation NH_3 (ND_3) exposure at 300 K.

Acknowledgments

This work was supported by the U.S. Office of Naval Research under Contract No. N00014-86-K-545. Some of the equipment utilized in this work was provided by the NSF-MRL through the Center for Material Research at Stanford University. We would like to thank Michael Y. Han for technical assistance. SMG acknowledges the National Science Foundation for a Presidential Young Investigator Award and the A.P. Sloan Foundation for a Sloan Research Fellowship.

References

[1] R.J. Hamers, Ph. Avouris and F. Bozso, Phys. Rev. Lett. **59**, 2071 (1987).

[2] Ph. Avouris, F. Bozso and R.J. Hamers, J. Vac. Sci. Technol. B5, 1387 (1987).

[3] R. J. Hamers, Ph. Avouris and F. Bozso, J. Vac. Sci. Technol. A6, 508 (1988).

[4] R. Wolkow and Ph. Avouris, Phys. Rev. Lett. **60**, 1049 (1988).

[5] Ph. Avouris and R. Wolkow, Phys. Rev. B **39**, 5091 (1989).

[6] S. Tanaka, M. Onchi and M. Nishijima, Surf. Sci. **191**, L756 (1987).

[7] D.G. Kilday and G. Margaritondo, D.J. Frankel, J.Anderson, and G.J. Lapeyre, Phys. Rev. B 35, 9364 (1987).

[8] M. Nishijima and K. Fujiwara, Solid State Commun. **24**, 101 (1977).

[9] T. Isu and K. Fujiwara, Solid State Commun. **42**, 477 (1982).

[10] E.K. Hlil, L. Kubler, J.L. Bischoff and D. Bolmont, Phys. Rev. B **35**, 5913 (1987).

[11] F. Bozso and Ph. Avouris, Phys. Rev. B **38**, 3937 (1988).

[12] J.L. Bischoff, L. Kubler and D. Bolmont, Surf. Sci. **209**, 115 (1989).

[13] B.G. Koehler, P.A. Coon, and S.M. George, J. Vac. Sci. Technol. B **7**, 1303 (1989).

[14] M.J. Dresser, P.A. Taylor, R.M. Wallace, W.J. Choyke and J.T. Yates Jr., Surf. Sci. **218**, 75 (1989).

[15] A.L. Johnson, M.M. Walczak and T.E. Madey, Langmuir **4**, 277 (1988).

[16] Y.J. Chabal, Phys. Rev. B **29**, 3677 (1984).

[17] P.A. Schumann Jr., W.A. Keenan, A.H. Tong, H.H. Gegenwarth and C.L. Schneider, J. Electrochem. Soc. **118**, 145 (1971).

[18] R.J. Collins and H.Y. Fan, Phys. Rev. **93**, 674 (1954).

[19] L.A. Pugh and K.N. Rao, *Molecular Spectroscopy:Modern Research*, edited by K.N. Rao (Academic, New York, 1976), Vol II.

[20] A. Uhlir, Bell Syst. Tech. J **35**, 333 (1956).

[21] D.R. Turner, J. Electrochem. Soc. **105**, 402 (1958).

[22] S.F. Chuang, S.D. Collins and R.L. Smith, Appl. Phys. Lett. **55**, 675 (1989).

[23] G. Bomchil, R. Herino, K. Barla and J.C. Pfister, J. Electrochem. Soc. **130**, 1161 (1983).

[24] K. Barla, R. Herino, G. Bomchil and J.C. Pfister, J. Cryst. Growth **68**, 727 (1984).

[25] V. Labunov, V. Bondarenko, L. Glinenko, A. Dorofeev and L. Jabulina, Thin Solid Films **137**, 123 (1986).

[26] M.I.J. Beale, J.D. Benjamin, M.J. Uren, N.G. Chew and A.G. Cullis, J. Cryst. Growth **75**, 408 (1986).

[27] K. Barla, R. Herino, G. Bomchil, J.C. Pfister and A. Freund, J. Cryst. Growth **68**, 727 (1984).

[28] I.M. Young, M.I.J. Beale and J.E. Benjamin, Appl. Phys. Lett. **46**, 1133 (1985).

[29] R.W. Hardman, M.I.J. Beale, D.B. Gasson, J.M. Keen, C. Pickering and D.J. Robbins, Surf. Sci. **152**, 1051 (1985).

[30] K. Barla, G. Bomchil, R. Herino and J.C. Pfister, J. Cryst. Growth **68**, 721 (1984).

[31] S. Konaka, M. Tabe and T. Sakai, Appl. Phys. Lett. **41**, 86 (1982).

[32] P. Gupta, V.L. Colvin and S.M George Phys. Rev. **37**, 8234 (1988).

[33] G. Shulze and M. Henzler, Surf. Sci. **124**, 336 (1983).

[34] B.G. Koehler, C.H. Mak, P.A. Coon, D.A. Arthur and S.M. George, J. Chem. Phys. **89**, 1709 (1988).

[35] P. Gupta, A.C. Dillon, A.S. Bracker and S.M. George, *submitted to Surface Science.*

[36] B.G. Koehler, C.H. Mak and S.M. George, Surf. Sci. **221**, 565 (1989).

[37] P. Gupta, A.C. Dillon, P.A. Coon and S.M. George, *submitted to Chem. Phys. Lett.*

[38] S.M. George, J. Vac. Sci. Technol. A **4**, 2394 (1986).

[39] G.E. Jellison, *Semiconductors and Semimetals:* Pulsed Laser Processing of Semiconductors; edited by R.F. Wood, C.W. White and R.T. Young (Academic Press, New York), Chapter 3, Vol III.

[40] G.G. MacFarlane, T.P. McLean, J.E. Quarrington and V. Roberts, Phys. Rev. **111**, 1245

(1958)

[41] H.A. Weakliem and D. Redfield, J. Appl. Phys. **50**, 1491 (1979).

[42] Y.J. Chabal and K. Raghavachari, Phys. Rev. Lett. **54**, 1055 (1985).

[43] Y.J. Chabal in *Semiconductor Interfaces: Formation and Properties* (Springer Verlag, NY 1987).

[44] F. Stucki, J.A. Schaefer, J.R. Anderson, G.J. Lapeyre and W. Gopel, Solid State Commun. **47**, 95 (1983).

[45] A. Marchand, M.T. Forel, F. Metras and J. Valade, J. Chim. Phys. **61**, 343 (1964).

[46] A. Lee Smith, Spectrochimica Acta **16**, 87 (1960).

[47] H. Kriegsmann, Z. Anorg. u. Allgem Chem. **298**, 223 (1959).

[48] H. Kriegsmann, Z. Elektrochem **61**, 1088 (1957).

[49] John Overend. in *Vibrational Intensities in Infrared and Raman Spectroscopy*, edited by W.B. Pearson and G. Zerbi (Elsevier Scientific Publishing Co., NY, 1982)

[50] E.A.V. Ebsworth, J.R. Hall, M.J. Mackillop, D.C. Mc Kean, N. Sheppard and L.A. Woodward, Spectrochimica Acta **13** 202, (1958).

[51] C. Mallot, H.Roulet, G.Dufour, J. Vac Sci. Technol. B **2**, 316 (1984).

[52] A.G. Schrott and S.C. Fain Jr., Surf. Sci. **123**, 223 (1982).

[53] K. Edamoto, S Tanaka, M. Onchi and M. Nishijima, Surf. Sci. **167**, 285 (1986).

[54] K. Nakamoto *Infrared and Raman Spectra of Inorganic and Coordination Compounds* (John Wiley & Sons, Inc., NY, 1986) Vol. IV.

Figure Captions

1. Infrared spectrum after a saturation NH_3 exposure on porous silicon surfaces at 300 K.

2. Infrared spectrum after a saturation ND_3 exposure on porous silicon surfaces at 300 K.

3. Infrared absorbance of a) the $SiN-H_2$ scissors mode and b) the Si-H stretching vibration as a function of annealing temperature after a saturation NH_3 exposure at 300 K.

4. Infrared absorbance of the Si_3-N vibrational modes as a function of annealing temperature after a saturation ND_3 exposure at 300 K.

5. Integrated infrared absorbances of the Si-H, $SiN-H_2$, $Si-NH_2$, and Si_3-N vibrational modes at 2077, 1534, 827 and 930, 750 cm^{-1}, respectively, as a function of annealing temperature after a saturation NH_3 exposure at 300 K.

6. Integrated infrared absorbances of the Si-D, $SiN-D_2$ and Si_3-N vibrational modes at 1510, 1157 and 930, 750 cm^{-1}, respectively, as a function of annealing temperature after a saturation ND_3 exposure at 300 K.

7. Integrated infrared absorbance of the Si-D stretching vibration at 1510 cm^{-1} as a function of ND_3 exposure on porous silicon surfaces at temperatures of 300, 400 and 600 K.

8. Integrated infrared absorbance of the $SiN-D_2$ scissors mode at 1157 cm^{-1} as a function of ND_3 exposure on porous silicon surfaces at temperatures of 300, 400 and 600 K.

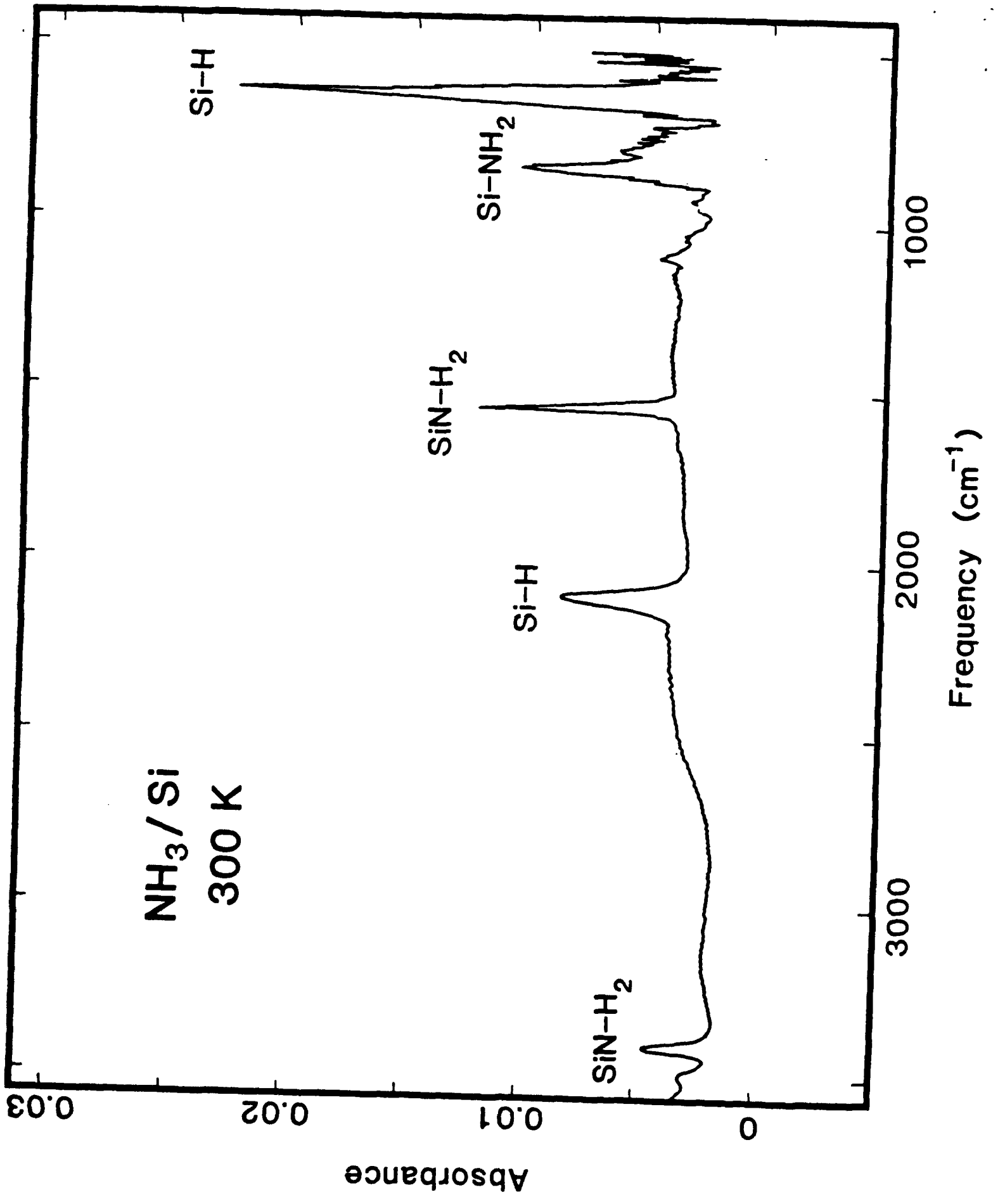
Si–H
Si–NH2
SiN–H2
Si–H
SiN–H2
NH3 / Si
300 K
Absorbance
0
0.01
0.02
0.03
1000
2000
3000
Frequency (cm-1)

Fig. 1

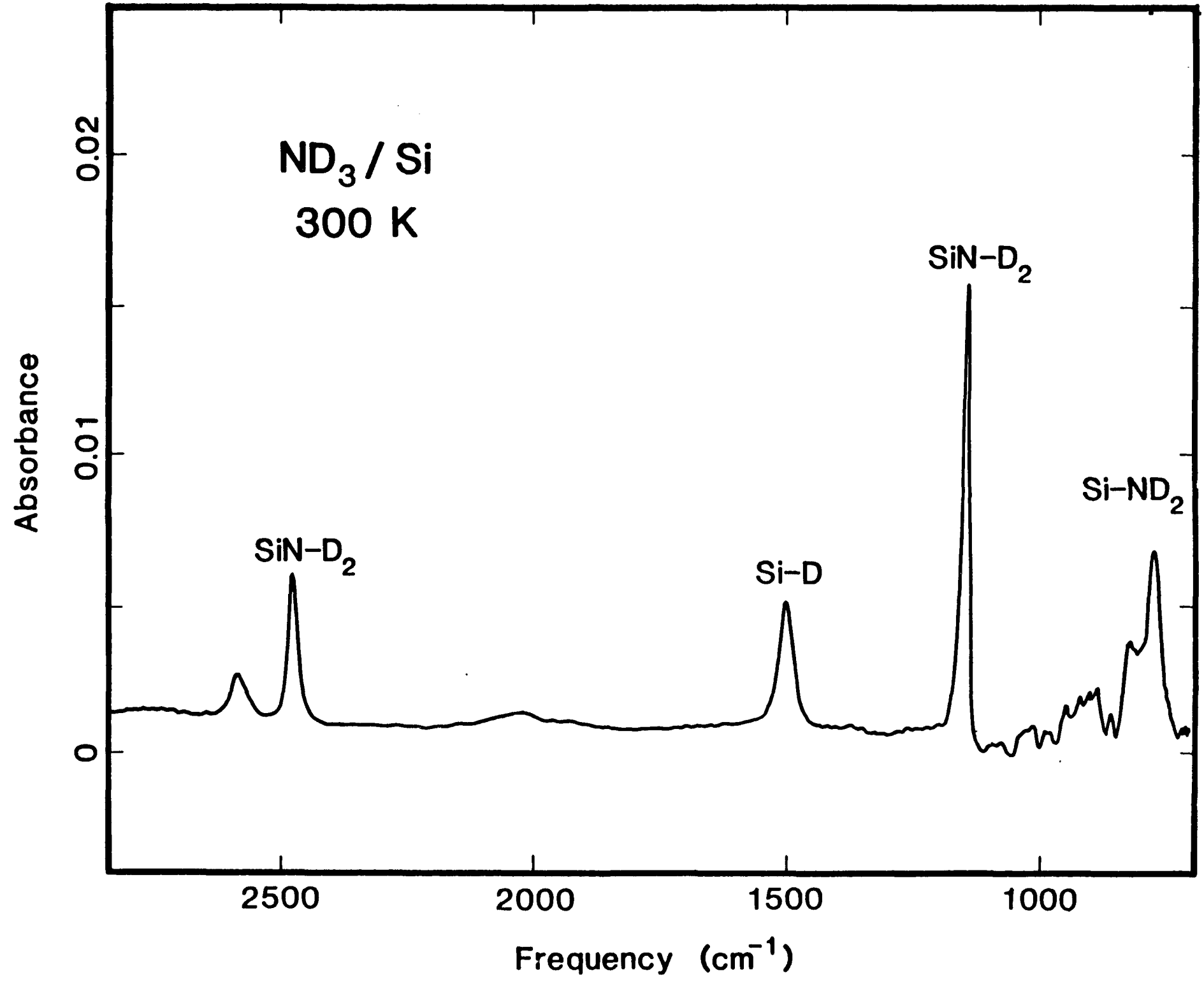
ND_3 / Si
300 K
SiN–D_2
Si–D
SiN–D_2
Si–ND_2
Absorbance
0.02
0.01
0
2500
2000
1500
1000
Frequency (cm^{-1})

Fig. 2

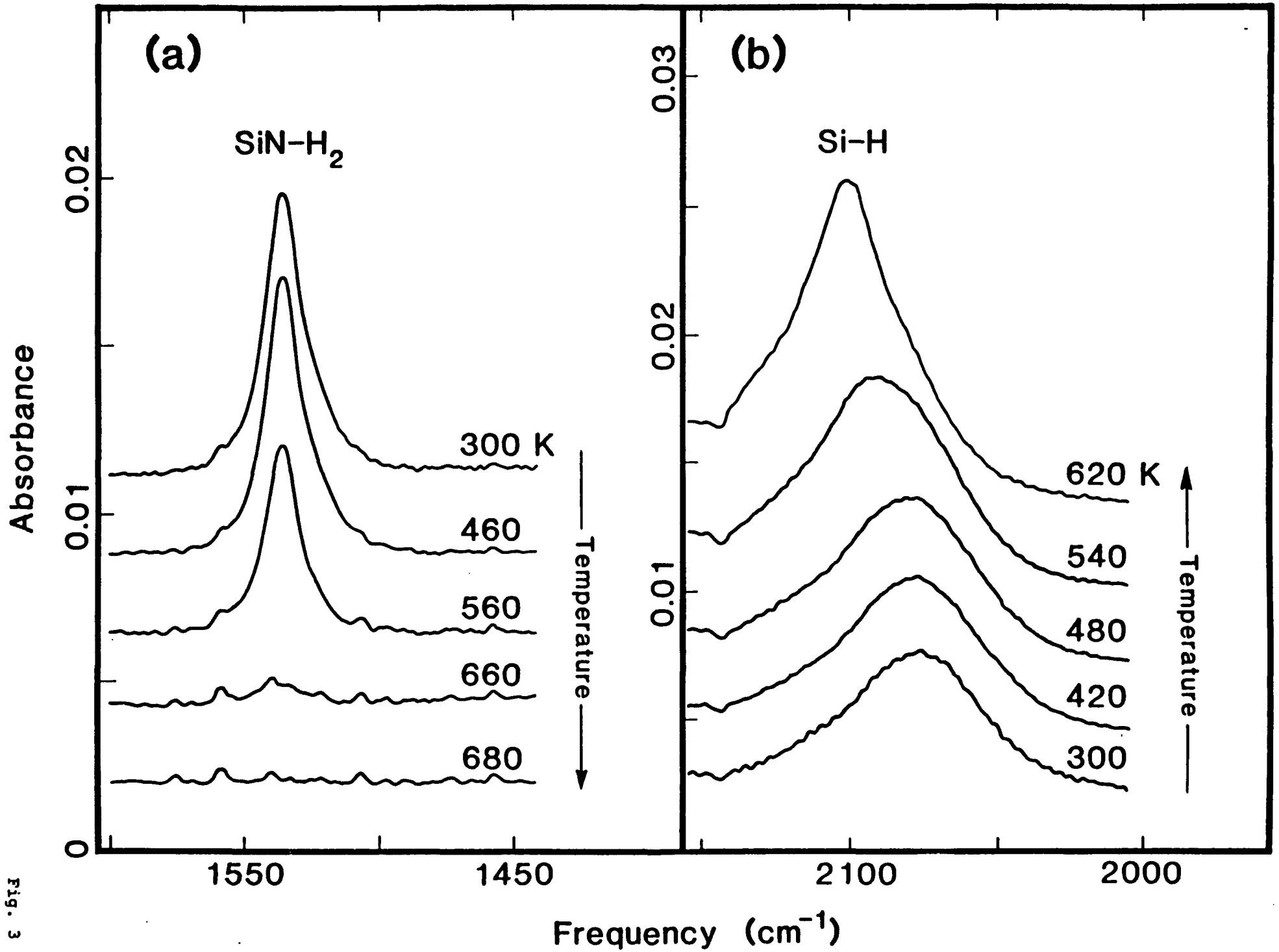
(a)
SiN–H2
0.02
0.01
0
300 K
460
560
660
680
Temperature
1550
1450
(b)
Si–H
0.03
0.02
0.01
620 K
540
480
420
300
Temperature
2100
2000
Absorbance
Frequency (cm−1)

Fig. 3

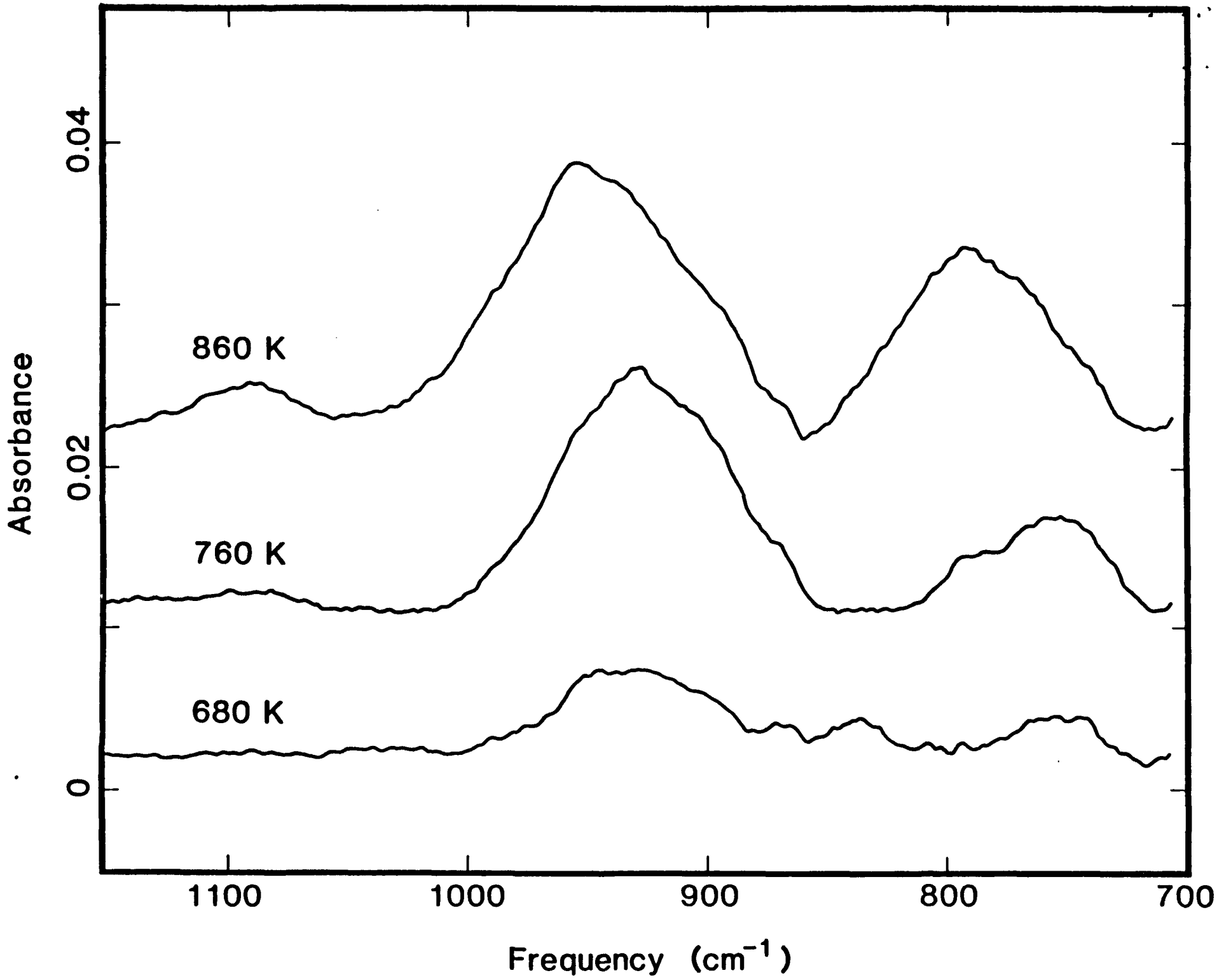
0.04
0.02
0
Absorbance
860 K
760 K
680 K
1100
1000
900
800
700
Frequency (cm^{-1})

Fig. 4

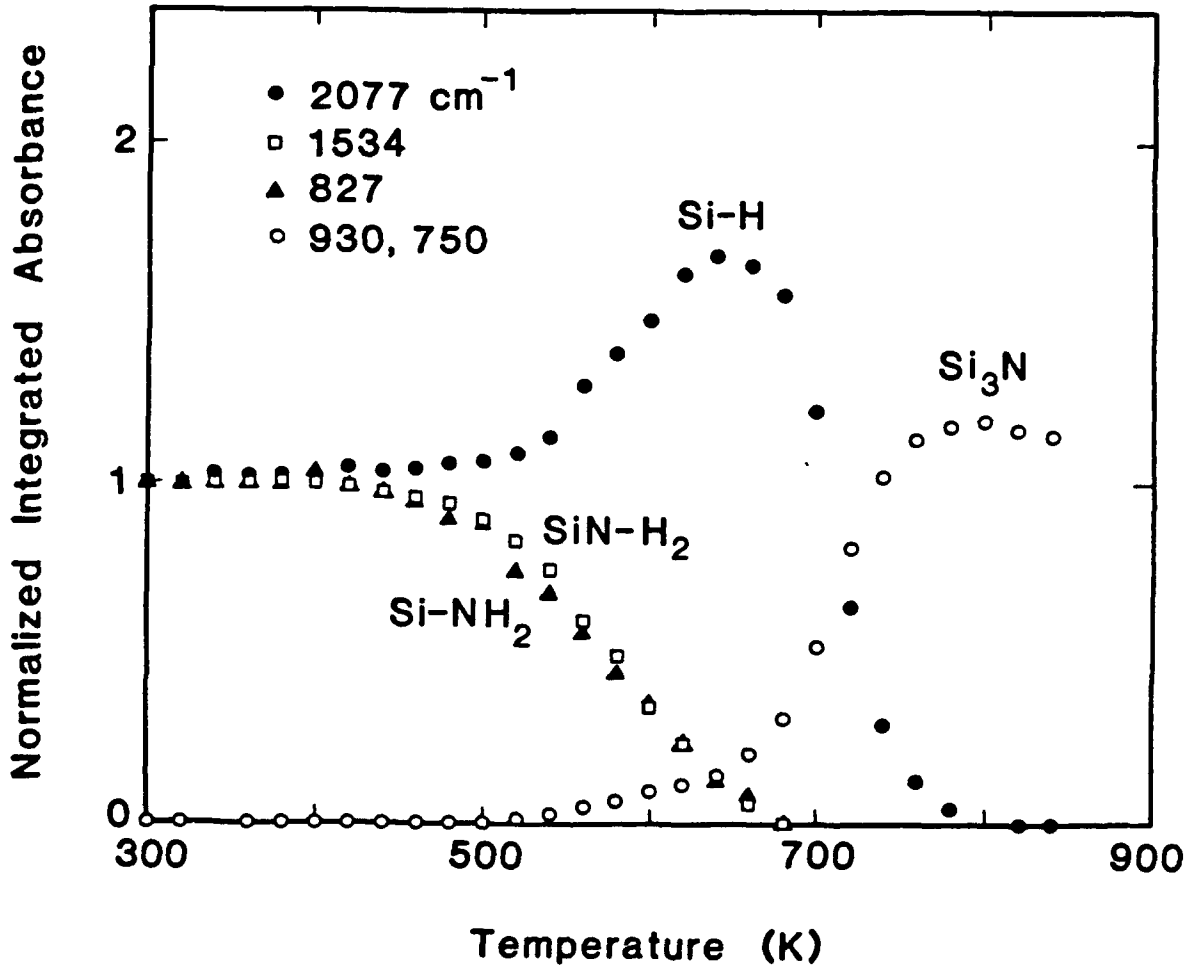
Normalized Integrated Absorbance
2077 cm^{-1}
1534
827
930, 750
Si-H
Si$_3$N
SiN-H$_2$
Si-NH$_2$
0
1
2
300
500
700
900
Temperature (K)

Fig. 5

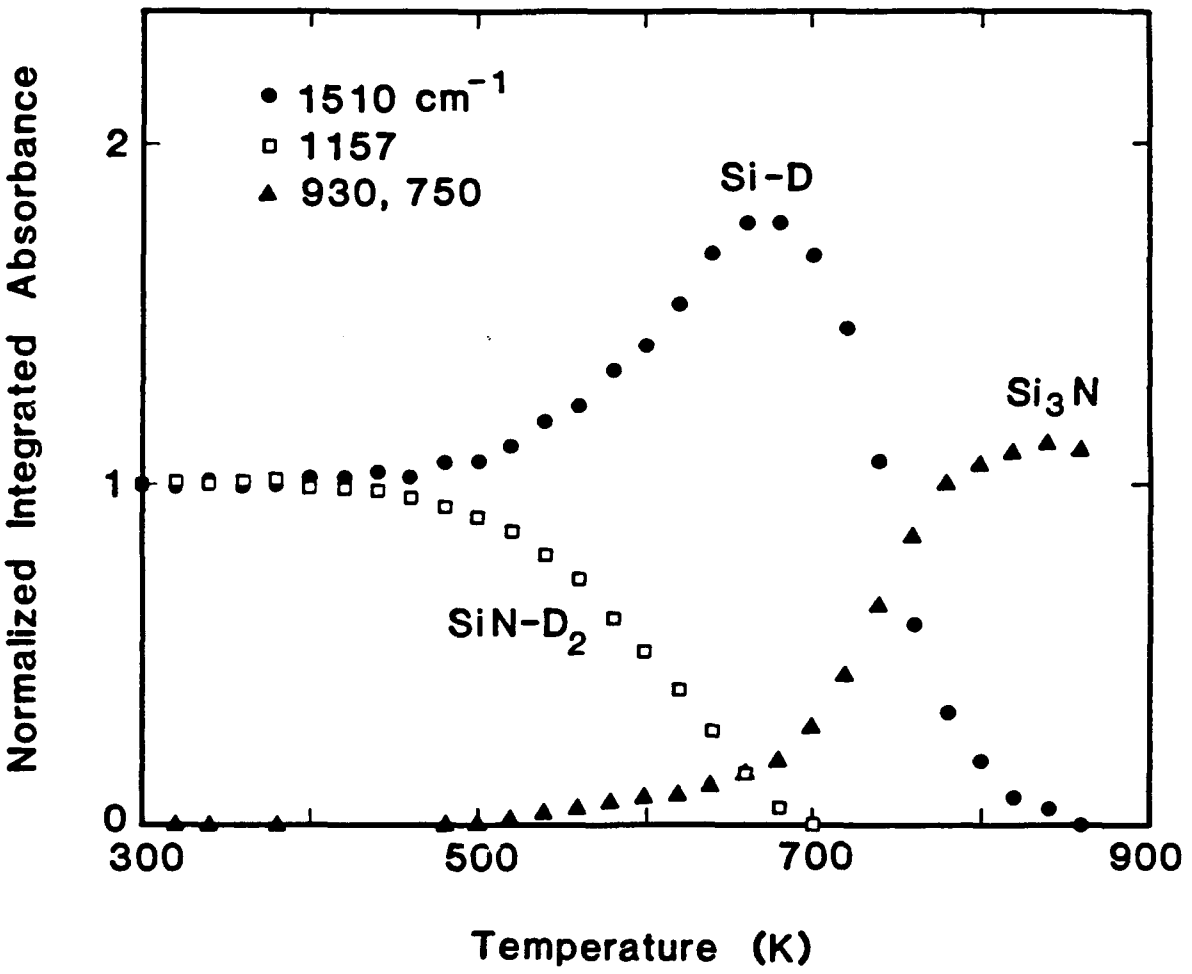
Normalized Integrated Absorbance
2
1
0
300
500
700
900
Temperature (K)
• 1510 cm^{-1}
▫ 1157
▲ 930, 750
Si-D
Si$_3$N
SiN-D$_2$

Fig. 6

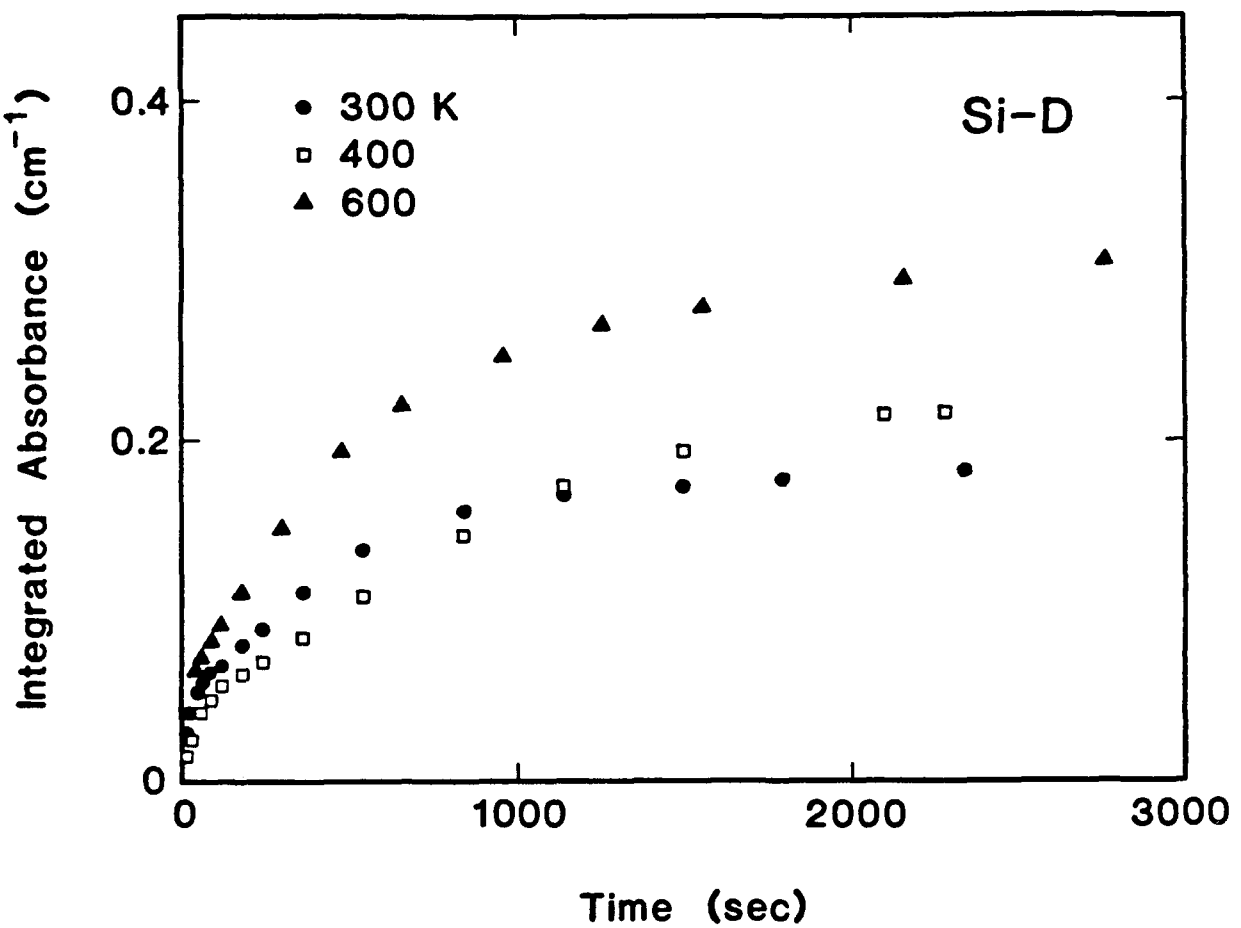
Integrated Absorbance (cm^{-1})
0.4
0.2
0
300 K
400
600
Si-D
0
1000
2000
3000
Time (sec)

Fig. 7

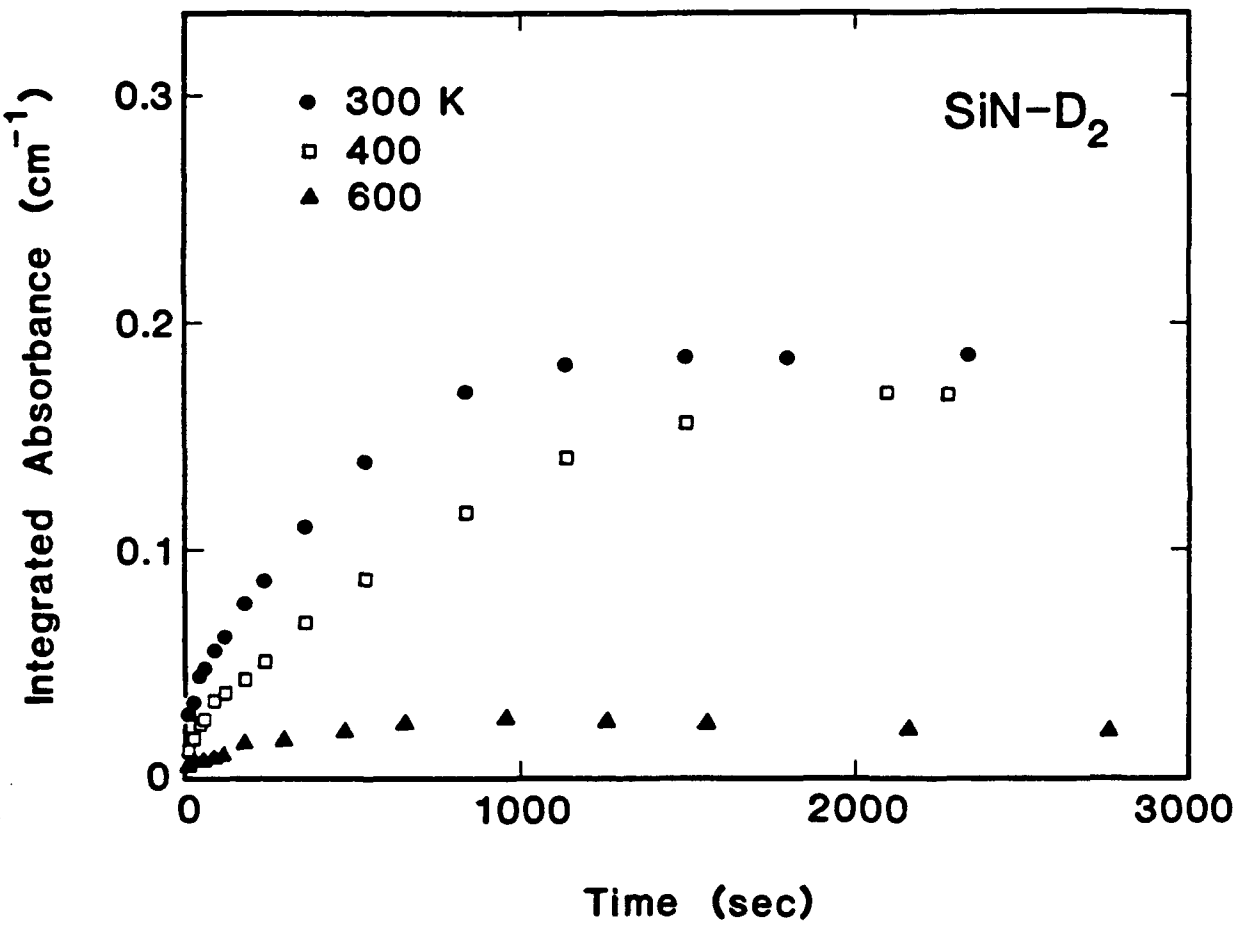
300 K
400
600
SiN-D2
Integrated Absorbance (cm-1)
0.3
0.2
0.1
0
0
1000
2000
3000
Time (sec)

Fig. 8